Journal of Catalysis 276 (2010) 314–326

Contents lists available at ScienceDirect

Journal of Catalysis

journal homepage: www.elsevier.com/locate/jcat

Carbon nanotube-supported Pt-based bimetallic catalysts prepared by a microwave-assisted polyol reduction method and their catalytic applications in the selective hydrogenation

Zhen Guo [a], Yuanting Chen [a], Lusi Li [a], Xiaoming Wang [b], Gary L. Haller [b], Yanhui Yang [a,*]

[a] School of Chemical and Biomedical Engineering, Nanyang Technological University, Singapore 637459, Singapore
[b] Department of Chemical Engineering, Yale University, New Haven, CT 06520, USA

ARTICLE INFO

Article history:
Received 23 July 2010
Revised 21 September 2010
Accepted 22 September 2010
Available online 20 October 2010

Keywords:
Bimetallic catalyst
Selective hydrogenation
Cinnamaldehyde
Close contact
Solvent effect
Carbon nanotubes

ABSTRACT

Platinum-based bimetallic catalysts supported on multi-walled carbon nanotube (CNT) were prepared by a facile microwave-assisted polyol reduction method (MAPR) and chemically probed in the selective hydrogenation of cinnamaldehyde. These bimetallic catalysts outperformed the catalysts prepared by the conventional impregnation method. CNT surface properties, selection of solvent and transition metal promoter were identified to be of great significance in tuning the catalytic performance. The best catalytic results were obtained on the Fe- and Co-modified Pt catalysts in the presence of ethyl acetate as the solvent after removing the oxygen-containing groups from CNT surfaces. Electrochemistry measurements including cyclic voltammetry and CO stripping, competitive hydrogenations of toluene and benzene, X-ray diffraction, X-ray photoelectron spectroscopy and transmission electron microscopy were employed to gain insights into the physicochemical properties of catalysts. Both catalytic reactions and characterizations revealed that the MAPR method afforded close contact between promoters and platinum active sites, leading to superior catalytic properties.

© 2010 Elsevier Inc. All rights reserved.

1. Introduction

Selective hydrogenation of unsaturated carbonyl compounds is of paramount importance in pharmaceutical and fragrance industries [1]. Selective hydrogenation of cinnamaldehyde (CALD) to cinnamal alcohol (CALC) is a representative example of such reactions. [2]. Nevertheless, hydrogenation of CALD forms other by-products such as hydrocinnamaldehyde (HALD) and hydrocinnamal alcohol (HALC) due to the thermodynamically favorable hydrogenation of C=C double bonds of α,β-unsaturated aldehydes [2,3]. In many cases, by-products such as acetals and other unidentified high molecular weight compounds may also be produced in large quantity [2,4]. Research efforts have been devoted to improve the selectivity toward the desired unsaturated alcohol CALC. Supported platinum nanoparticles have been extensively investigated and appear to be the most effective catalysts for the selective hydrogenation of CALD [1,5,6].

Recent studies have focused on the effects of supports and promoters on the activity and selectivity of Pt metallic nanoparticles in CALD selective hydrogenation. Different support materials may lead to distinctive hydrogenation results due to the specific interactions between support and Pt nanoparticles [7]. The catalytic performance of metallic nanoparticles may also be drastically changed by modifying the surface chemistry of the support, e.g., the activity of Pt nanoparticles was enhanced by a factor of 25 after removing the surface oxygen-containing groups from a carbon nanofiber (CNF) support [8]. Another promising approach to enhance the catalytic properties of Pt nanoparticles is to introduce a second metal (or metal oxide) to form bimetallic catalysts. It has been reported that metal promoters, such as Ga [8], Co [9] and Ru [10], play a vital role in CALD hydrogenation in the presence of supported Pt nanoparticles due to the synergetic interactions between Pt active sites and promoters.

In addition to support and promoter, other factors, e.g., the preparation method, may also affect the outcome of selective hydrogenation. Several methodologies have been developed to synthesize Pt-based bimetallic catalysts. Although the procedures of ion-exchange and impregnation (IMP) methods are simple, the activities of as-synthesized catalysts are usually poorer when compared to the catalysts prepared by more sophisticated approaches, such as homogeneous deposition precipitation (HDP) and reductive deposition precipitation (RDP) [8]. For the RDP method, hydrogen is adsorbed on the pre-reduced parent metallic catalyst, followed by depositing promoters on the pre-formed metal nanoparticles via the reduction of promoter precursors by the adsorbed hydrogen [11]. The successive reduction steps in RDP result in close contact between promoters and main active centers, which

* Corresponding author. Fax: +65 6794 7553.
E-mail address: yhyang@ntu.edu.sg (Y. Yang).

0021-9517/$ - see front matter © 2010 Elsevier Inc. All rights reserved.
doi:10.1016/j.jcat.2010.09.021

affords favorable catalytic properties in selective hydrogenation [8]. Recently, a novel preparation method, i.e., microwave-assisted polyol reduction (denoted as MAPR) technique has been proposed to synthesize Pt-based electro-catalysts for fuel cells [12,13]. Microwave irradiation allows uniform heating of the metal precursors to a high temperature within a few seconds, leading to a shorter crystallization time and more homogenous nucleation when compared to conventional preparation methods [13].

In this contribution, we apply this facile MAPR method to prepare Pt-based bimetallic catalysts with high activity and selectivity for CALD hydrogenation, superior to those catalysts synthesized by the conventional IMP method. The effects on the catalytic performance of as-prepared bimetallic catalysts due to the pretreatment of multi-walled carbon nanotube (CNT) support surfaces, solvents and transition metal (metal oxide) promoters are examined. In addition to the conventional characterization techniques such as X-ray diffraction (XRD), X-ray photoelectron spectroscopy (XPS) and transmission electron microscopy (TEM), competitive hydrogenations of toluene and benzene are employed to chemically probe the electron density of Pt nanoparticles. We also apply the electrochemistry measurements including cyclic voltammetry (CV) and CO stripping to identify the nature of as-prepared bimetallic catalysts. It is revealed that different from IMP method, MAPR retains the hydrophobic surface properties of CNT and affords close contact between promoters and Pt nanoparticles, e.g., metal–metal electronic interaction, which significantly improves the catalytic performance of Pt active sites. Interestingly, other than generally adopted solvents such as alcohols [1,2] and alkanes [14], the as-prepared catalysts in this study showed remarkably high activity and selectivity in the presence of ethyl acetate (EA) as the solvent.

2. Materials and methods

2.1. Chemicals

$H_2PtCl_6{\cdot}6H_2O$ (>37.5% Pt basis, Sigma–Aldrich), $Mn(NO_3)_2{\cdot}4H_2O$ (>97%, Sigma–Aldrich), $Fe(NO_3)_3{\cdot}9H_2O$ (>98%, Sigma–Aldrich), $Co(NO_3)_2{\cdot}6H_2O$ (>98%, Sigma–Aldrich), $Ni(NO_3)_2{\cdot}6H_2O$ (>98.5%, Sigma–Aldrich), $Cu(NO_3)_2{\cdot}2.5H_2O$ (98%, Sigma–Aldrich), $Zn(NO_3)_2{\cdot}6H_2O$ (>98%, Sigma–Aldrich), $SnCl_2$ (98%, Sigma–Aldrich), HNO_3 (65%, Fluka), KOH (99.99%, Sigma–Aldrich), CaH_2 (95%, Sigma–Aldrich), ethylene glycol (EG, 99.5%, Sinopharm. Chemical Reagent), Nafion solution (5% in isopropanol and water, Sigma–Aldrich), CALD (>99%, Aldrich), tetradecane (>99.5%, Fluka), cyclohexane (99.5%, Sigma–Aldrich), 1-butanol (>99%, Sigma), ethanol (>99.5%, Sigma–Aldrich), 2-propanol (>99%, Sigma), EA (>99.5%, Acros), 1,4-dioxane (99.8%, Sigma–Aldrich), benzene (>99.9%, Sigma–Aldrich) and toluene (>99.9%, Sigma–Aldrich) were used as received without any further purification.

2.2. Synthesis

The pristine CNT (>95%, Cnano) was treated with concentrated and diluted nitric acids successively following the procedures as described by Lordi et al. [15]. The concentrated nitric acid removed the amorphous carbonaceous and metallic impurities; the diluted nitric acid slowly oxidized the purified CNT to create abundant surface functional groups, which facilitated the uniform deposition of metal precursors. To deposit Pt precursors onto functionalized CNT, 0.1 g of CNT was immersed in 722 μL of $H_2PtCl_6{\cdot}6H_2O$ aqueous solution (20 mg/mL) and dried at 373 K in vacuum. EG (40 mL) was added to the above-mentioned Pt–CNT composite followed by sonicating for 10 min to afford a homogenous suspension. The said suspension was transferred into a three-neck flask with a condenser and placed in a microwave reactor (Sineo, MAS-II). The slurry was agitated by a magnetic stirrer, and the temperature inside the flask was monitored by an infrared sensor. The suspension was heated to 438 K in 0.5 min and kept at the same temperature for 1.5 min. After cooling to room temperature, the powder was filtrated and washed with deionized water, followed by drying at 373 K in vacuum. The as-synthesized catalyst was denoted as Pt/CNT and the expected Pt loading is 5 wt.% and confirmed by inductively coupled plasma (ICP) measurements. Pt/CNT was pretreated at various temperatures (673, 773, 873 and 973 K) in a nitrogen flow (20 mL/min) for 2 h to remove the oxygen-containing groups from CNT surfaces. The resulting catalysts were denoted as Pt/CNT-673, Pt/CNT-773, Pt/CNT-873 and Pt/CNT-973.

The preparations of bimetallic catalysts were similar to that of Pt/CNT but in the presence of both Pt and transition metal precursors. The Pt loading was kept at 5 wt.%, and the molar ratio of Pt to promoter was 1:1. All the as-synthesized bimetallic catalysts were pretreated at 973 K in nitrogen and were denoted as PtMn/CNT-973, PtFe/CNT-973, PtCo/CNT-973, PtNi/CNT-973, PtCu/CNT-973, PtZn/CNT-973 and PtSn/CNT-973. For comparison, Pt/CNT catalysts promoted with Fe or Co were also prepared by a conventional IMP method (denoted as PtFe/CNT-973-IMP and PtCo/CNT-973-IMP). Aqueous solutions of $H_2PtCl_6{\cdot}6H_2O$ and $Fe(NO_3)_3{\cdot}9H_2O$ ($Co(NO_3)_2{\cdot}6H_2O$) were impregnated onto the oxidized CNT followed by drying under ambient conditions overnight. The impregnated catalysts were pre-reduced in a hydrogen flow (50 mL/min) at 473 K for 2 h and subsequently exposed to a nitrogen flow (20 mL/min) at 973 K for another 2 h.

2.3. Selective hydrogenation of CALD

Selective hydrogenation of CALD was carried out in a stainless steel reactor with Teflon liner (Parr 4950, controller 4843). A certain amount of catalyst (0.01 g), 0.2 g of CALD (1.5 mmol) and 7.25 mL of solvent were added into the reactor. Tetradecane (38 μL, 0.146 mmol) was added as an internal standard. The air residue inside the reactor was expelled by pressurizing and releasing hydrogen several times. The reaction was performed at 333 K under 10 atm of hydrogen for either 1 or 0.5 h depending on the catalyst activity. In order to eliminate the external mass transfer limitation, the effect of stirring speed on CALD conversion was studied. The results show that CALD conversion is constant when the stirring speed is above 600 rpm, denoting a kinetics-controlled regime (see Supporting information Fig. S-1). Thus, the stirring speed was set at 600 rpm for all the experiments in this study. After the reaction, the catalyst powder was filtered off, and the filtrate was analyzed using a gas chromatograph (Agilent, 6890 N) equipped with a HP-5 column (Agilent) and flame ionization detector (FID). The by-products were identified by a gas chromatography–mass spectrometry (GC–MS, Agilent, GC 6890 N, MS 5973 inert).

2.4. Characterizations

Powder XRD patterns were recorded on a Bruker AXS D8Focus diffractometer using a Ni filtered Cu Kα radiation (λ = 0.15406 1 nm), operated at 40 kV and 40 mA. Diffraction data were collected between 20° and 80° (2θ) with a resolution of 0.02° (2θ). TEM measurements were taken on a JEOL JEM-2010 operated at 200 kV. The samples were suspended in ethanol and dried on holey carbon-coated Cu grid. XPS measurements were taken on a VG Escalab 250 spectrometer equipped with an Al anode (Al Kα = 1846.6 eV). The background pressure in the analysis chamber was lower than 1×10^{-7} Pa. Measurements were taken using 20 eV pass energy, 0.1 eV step and 0.15 min dwelling time. Binding

energy correction was carried out using the C_{1s} peak of adventitious C at 284.6 eV.

CV and CO stripping voltammetries were carried out in a 1.0 M KOH solution at 50 mV s^{-1} (Princeton Applied Research, VersaSTAT 3 Potentiostat/Galvanostat). The working electrode was prepared by dropping 30 μL of the catalyst ink onto a glassy carbon electrode. The ink was prepared by ultrasonically mixing 2 mg of catalyst sample with 3 mL of 0.025 wt.% Nafion in ethanol solution. Pt foil and Hg/HgO (1.0 M KOH) electrodes were used as the counter and reference electrodes, respectively. All the potentials in the present study are given vs. the Hg/HgO (1.0 M KOH) electrode. The potentials of CV test ranged between −0.8 and 0.3 V. CO stripping was performed as follows: after purging the solution with nitrogen for 20 min, gaseous CO was bubbled for 15 min to form the CO adlayer on the catalysts while maintaining the potential at −0.8 V. Excess CO in the solution was expelled by purging with nitrogen. CO stripping voltammetry was also recorded in a range between −0.8 and 0.3 V.

Competitive hydrogenations of toluene and benzene were carried out to probe the electronic properties of Pt nanoparticles. By measuring the relative hydrogenation rates of toluene and benzene, an equilibrium adsorption constant ($K_{T/B}$) can be derived from Eq. (1), in which P_T/P_B is the ratio of toluene to benzene partial pressures, r_B^0 is the reaction rate of pure benzene, r_B is the reaction rate of benzene at P_T/P_B [16]. $K_{T/B}$ is temperature dependent, and its value is related to the electron deficiency of Pt nanoparticles; the larger the $K_{T/B}$ value, the more electron deficient is the Pt [17].

$$r_B^0/r_B = 1 + K_{T/B}(P_T/P_B) \quad (1)$$

The procedures for toluene and benzene hydrogenations were similar to that reported by Poondi and Albert Vannice [16]. A liquid chromatography pump (Shimadzu, LC-20AT) introduced toluene and benzene into a mixer maintained at 423 K. The ratios of toluene/benzene ranged from 0 to 0.8. The gasified aromatic mixture was carried by a H_2 flow (40 mL/min) and passed through 0.02 g of catalyst pre-loaded in a down-flow quartz reactor. The reactor temperature was maintained at 308 K. The effluent gas was analyzed using an online gas chromatograph (Agilent, 6890 N) fitted with a HP-PONA column (Agilent) and FID detector. All the reaction conversions were kept below 10%.

3. Results

3.1. Effects of CNT surface oxygen-containing groups

Catalyst support may influence hydrogenation via steric or electronic interaction, which is usually contributed by the surface properties of support material [3]. The surface oxygen-containing groups on a carbonaceous support including carboxylic, carbonyl and hydroxyl moieties are initially indispensable to enhance the loading and dispersion of metal precursors [13]. Interestingly, removal of these oxygen-containing groups from CNF [18] surfaces by a high-temperature treatment after loading metal particles remarkably increases both selectivity and activity in hydrogenation. Toebes et al. reported the correlation between the surface oxygen density and the performance of CALD hydrogenation over a CNF-supported Pt catalyst [19]. They suggested that the oxygen-containing groups could be effectively removed from carbonaceous surfaces when the annealing temperature was higher than 573 K. Herein, the effects of CNT surface oxygen-containing groups on hydrogenation performances over the catalysts prepared by MAPR were examined. Pt/CNT catalysts were pretreated in a temperature ranged from 673 to 973 K in nitrogen.

Various techniques, including XPS, Boehm titration, thermogravimetric analysis (TGA) and chemical derivatization, have been employed to characterize the functional groups bonded on CNF [19] and CNT [20] surfaces. In this study, the density of surface oxygen-containing groups on CNT was related to their electrochemical properties. CV measurements were taken on Pt/CNT catalysts, and the results are shown in Fig. 1a. As the pretreatment temperature increases, a remarkable decrease in the area enclosed by CV curves, i.e., the background of CV signal is observed. Similar result is also obtained for pure CNT before and after high-temperature annealing in an inert atmosphere (see Supporting information Fig. S-2). The decrease in area enclosed by CV curves has been reported by Lawrence et al. [21]. In their study, CV profiles of CNT prepared by different methods (including arc discharge

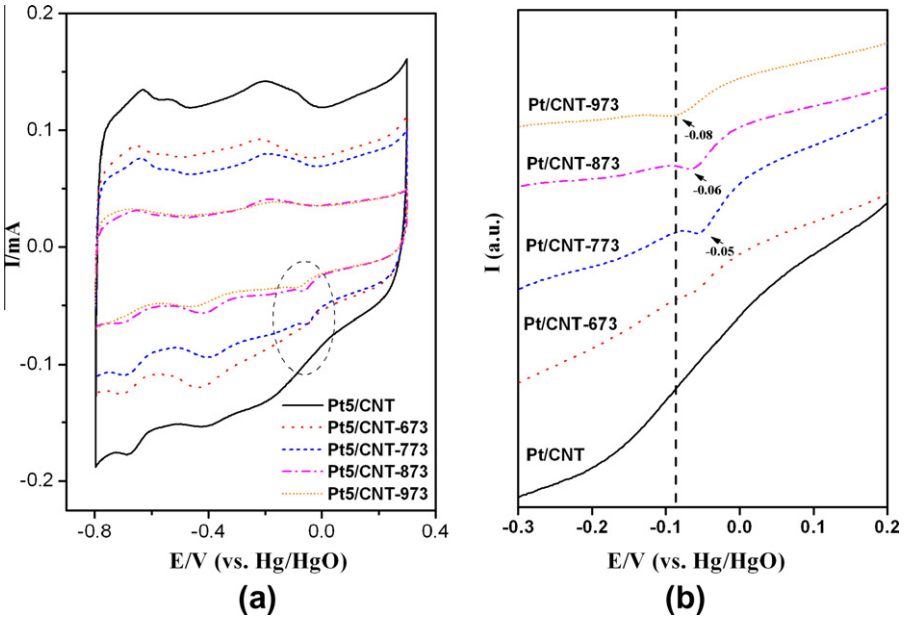

Fig. 1. (a) Cyclic voltammograms (CVs) of Pt/CNT catalysts in 1 M KOH solution with a scan rate of 50 mV s^{-1}; (b) magnification of the circled area in (a) showing shift of Pt–O reduction peaks.

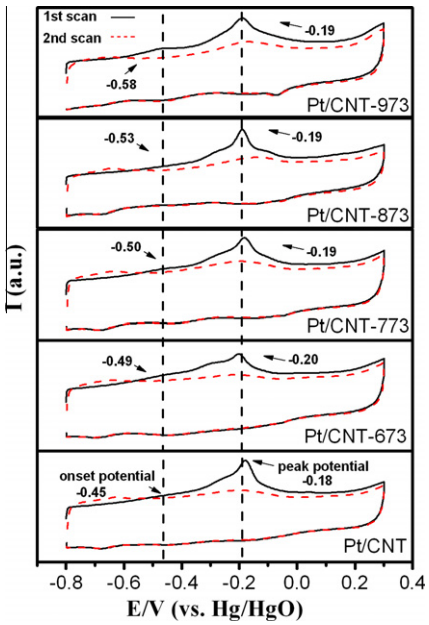

Fig. 2. CO stripping voltammograms of Pt/CNT catalysts treated with different temperatures. The left and right dash lines indicate the onset and peak potentials of Pt/CNT, respectively.

and chemical vapor deposition) were assessed, and they suggested that a larger quantity of redox active sites (e.g., quinone) on CNT surfaces led to a larger capacitance and CV background. A similar trend was also observed on the carbon black pretreated in HNO_3 with different concentrations and pretreatment time durations [22]. Boiling carbon black in a concentrated HNO_3 solution for 18 h resulted in the elimination of surface oxygen-containing groups (such as quinone and hydroquinone) and consequently a small area enclosed by the CV curves. Therefore, the decrease in CV background upon high-temperature annealing observed in this study suggests the removal of oxygen-containing groups from CNT surfaces.

In these CV profiles, redox peak signals at *ca.* −0.7 and −0.5 V are contributed by the adsorption and desorption of hydrogen atoms bonded on Pt surface [23]. These peaks become less pronounced at higher annealing temperatures, implying the decrease in Pt surfaces areas, i.e., enlargement of the Pt particle sizes. Due to the low Pt loading, the platinum oxide (Pt–O) reduction peaks [24] are only discernable for Pt/CNT-773, Pt/CNT-873 and Pt/CNT-973 with low backgrounds as shown in Fig. 1b, which is the magnification of circled area in Fig. 1a. The reduction potential depends on the thermodynamics of metal oxide, kinetics of all involved reduction steps and the electrochemical environment [25]. In an alkaline solution, Pt–O reduction follows the steps [23]:

$$Pt - O + H_2O + e^- \rightarrow Pt - OH + OH^- \quad (2)$$

$$Pt - OH + e^- \rightarrow Pt + OH^- \quad (3)$$

The Pt–O reduction potential decreases with increasing pretreatment temperature, implying that low density of surface oxygen-containing groups hampers the Pt–O reduction. Removal of surface oxygen increases the hydrophobicity of CNT surfaces, which hinders the contact of water with CNT support, resulting in a slow Pt–O reduction. Although a low density of surface oxygen-containing groups leads to a high conductivity of CNT [10], which may enhance the current flow in response to the applied potential (i.e., accelerate the diffusion of electrons to Pt particles) and result in a positive shift of the Pt–O reduction potential, the water accessibility to CNT, i.e., the hydrophobicity of support material plays a more important role in this particular reduction step.

CO stripping voltammetry is measured to characterize the catalysts with and without high-temperature pretreatment. In CO stripping, CO initially adsorbed on Pt nanoparticles will be oxidized to CO_2 at a negative potential along with the positively sweeping potential of the working electrode. The potential for CO oxidization relies on the electrochemical properties and chemical environment of Pt nanoparticles. In addition, compared to CV measurement, CO stripping is a more feasible method to determine the electrochemical active surface (EAS) areas of Pt nanoparticles when Pt loading is low, due to the low electrical signals attributed to the desorption of hydrogen atoms bonded on Pt surfaces and the uncertainty introduced by the background current subtraction [26]. Fig. 2 shows the CO stripping voltammograms of catalysts pretreated under different temperatures. The main peak potential for CO oxidization remains constant for all the catalysts, whereas the onset potential, at which CO stripping current attains 10% of the current at main peak potential [26], negatively shifts when the pretreatment temperature increases, suggesting that CO is more easily oxidized on catalyst surfaces with fewer oxygen-containing groups. It was reported that the oxidization of CO adsorbed on Pt–Ru nanoparticles supported on pristine CNT was easier when compared to the partially oxidized CNT, and the promoted CO elimination was assisted by the high conductivity of pristine CNT [27]. Vu et al. reported that the conductivity of a pristine CNT pellet is 1.5 times higher than that of CNT pretreated with HNO_3 [10]. Thus, the negative shift of CO oxidization peak is contributed by the improved conductivity of CNT after removing the surface oxygen-containing groups. The EAS areas of Pt nanoparticles were calculated based on the CO stripping voltammetry, assuming that the oxidation of a CO monolayer adsorbed on 1 cm^2 of Pt requires 420 μC [26]. The results show that the CO active surface areas of Pt sites decrease (see Table 1), implying the sintering of small Pt nanoparticles at high temperatures. These observations were further evidenced by XRD and TEM measurements.

Fig. 3a shows the XRD patterns of Pt/CNT catalysts pretreated in a nitrogen flow under different temperatures. The strong (0 0 2) diffraction of hexagonal graphite at 2θ of 25.8° suggests that the graphite structure of CNT is retained after oxidizing CNT in HNO_3, depositing Pt precursors under microwave irradiation and subsequently pretreating at high temperatures [28]. The diffraction peaks at 2θ of 39.7°, 46.2° and 67.4° are attributed to the cubic platinum metal structure [29]. The average diameters of Pt nanoparticles (calculated based on the full width at half maximum of Pt(1 1 1) reflection using Scherrer's equation [28]) increase from 3 to 5 nm upon the high-temperature pretreatment, as listed in Table 1. The CO stripping and XRD results are in good agreement with direct TEM observations on Pt/CNT and Pt/CNT-973 as shown in Fig. 4a and b. Pt/CNT shows a mean particle size at around 3.7 nm with a narrow size distribution. A noticeable particle size increment is observed, and the particle size distribution is substantially wider after pretreating Pt/CNT at 973 K. The aggregation of Pt nanoparticles caused by the high-temperature pretreatment in this study is more noticeable than that of the carbon-supported Pt nanoparticles prepared by either IMP or HDP method [10,19]. For MAPR, Pt is reduced in the liquid phase, the nucleation and growth of Pt nanoparticles may take place either in the EG solution or on the CNT surfaces. Although the latter case is preferable due to the ionic interaction between CNT surface groups and Pt precursors [30], it is still arbitrary to preclude the possibility that Pt particles initially form in EG followed by adsorbing onto CNT surfaces, as nanosized noble metal particles can be formed in EG solutions in the absence of any support [12]. Meanwhile, the nucleation and growth of Pt nanoparticles occur primarily on CNT surface for IMP or HDP approach. It was reported that CNT-supported metal

Table 1
Hydrogenation results of CALD over Pt/CNT with different temperature treatments by using 2-propanol as solvent.

Catalysts	Particle size[a] (nm)	EAS[b] ($m^2\ g^{-1}$)	Conversion (%)	Yield of products (mol.%)				TOF[d] (h^{-1})
				CALC	HALD	HALC	Others[c]	
Pt/CNT	3.1	54.0	62.7	0	2.4	0	97.6	1213
Pt/CNT-673	4.5	31.0	37.2	0	5.2	0	94.8	1253
Pt/CNT-773	4.9	29.4	38.6	0	7.6	0	92.4	1371
Pt/CNT-873	5.2	22.6	53.5	43.5	7.1	0	49.4	2473
Pt/CNT-973	5.1	23.0	49.6	55.1	4.6	0	40.3	2288

[a] Particle sizes were calculated from XRD patterns of Pt based on Scherrer's equation.
[b] EAS areas were deduced from data of CO stripping.
[c] Based on the characterization of GC–MS, the other by-products include 1-(3-propoxyprop-1-enyl)benzene, cinnamyl formate, cinnamic acid, benzyl cinnamate, 4,4-diphenylcyclohexa-1,5-dienyl acetate and some condensation products which cannot be identified by our GC–MS due to their large molecular weights.
[d] TOF is defined as the number of converted CALD molecules in 1 h over one active site; the number of active sites (Pt atoms exposed on the surface of particles) is determined by EAS value. Reaction time is 1 h.

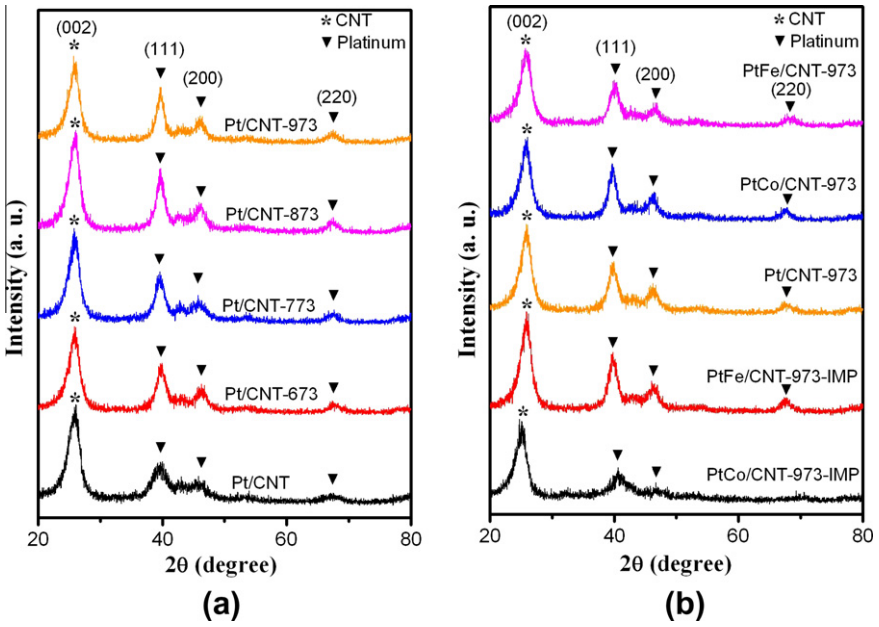

Fig. 3. (a) XRD patterns of Pt/CNT treated with different temperatures; (b) XRD patterns of PtFe/CNT-973, PtCo/CNT-973, Pt/CNT-973, PtFe/CNT-973-IMP and PtCo/CNT-973-IMP.

nanoparticles can catalyze the localized gasification of carbon when the sample was pretreated at a high temperature, giving rise to the formation of nanoscaled ridges and cavities (docking stations) on CNT surfaces, which may play an anchoring role in facilitating the immobilization of metal nanoparticles [31]. Therefore, the mobility of Pt nanoparticles on CNT surfaces prepared by MAPR is higher than that of CNT-supported Pt nanoparticles synthesized by IMP or HDP, resulting in a remarkable increase in the Pt nanoparticle size under a high-temperature pretreatment. Nevertheless, an optimized utilization of Pt active sites may be achieved under such circumstances because the interaction between support and Pt nanoparticles is minimized to a large extent [32,33].

To compare the catalytic properties of Pt/CNT pretreated at different temperatures, selective hydrogenation of CALD was conducted in 2-propanol (a commonly used solvent), and the results are listed in Table 1. For Pt/CNT pretreated at relatively low temperatures (673 and 773 K), CALD conversion dramatically decreases when compared to the pristine Pt/CNT, which may be attributed to the increased Pt particle size, i.e., diminishing of the available Pt active sites evidenced by EAS area measurements. Further increasing the annealing temperature leads to the elevation of conversion though the Pt particle size slightly increases. The CNT surface with a low oxygen density is beneficial for the π–π interaction between aryl ring of CALD and the basic π sites on CNT surfaces [10]. Therefore, the local concentration of CALD on CNT surfaces increases, resulting in an enhanced catalytic activity (as shown in Scheme 1a). The turnover frequency (TOF, calculated based on EAS areas) monotonically increases with the pretreatment temperature, suggesting the beneficial effect of removing surface oxygen from CNT support. TEM image shows that the Pt nanoparticle sizes remain essentially constant after the hydrogenation reaction (see Fig. 4c).

The effect of pretreatment temperature on selectivities is also distinct. When the catalysts supported on CNT with relatively high densities of surface oxygen-containing groups (Pt/CNT, Pt/CNT-673 and Pt/CNT-773) are tested, the product distributions are dominated by undesired compounds which are not derived from CALD hydrogenation but from side reactions, such as aldol condensation, oxidization and esterification [2,19]. These by-products have been identified using GC–MS and listed in the footnotes of Table 1. Toebes et al. suggested that these side reactions were acid-catalyzed; removing oxygen-containing groups from CNT surfaces decreased the acidity of CNT surfaces, which suppressed the formation of these by-products [19]. Unlike IMP and HDP preparation methods, in which the surface oxygen-containing groups on carbon supports may be partially removed after pre-reducing the catalyst in H_2 at a

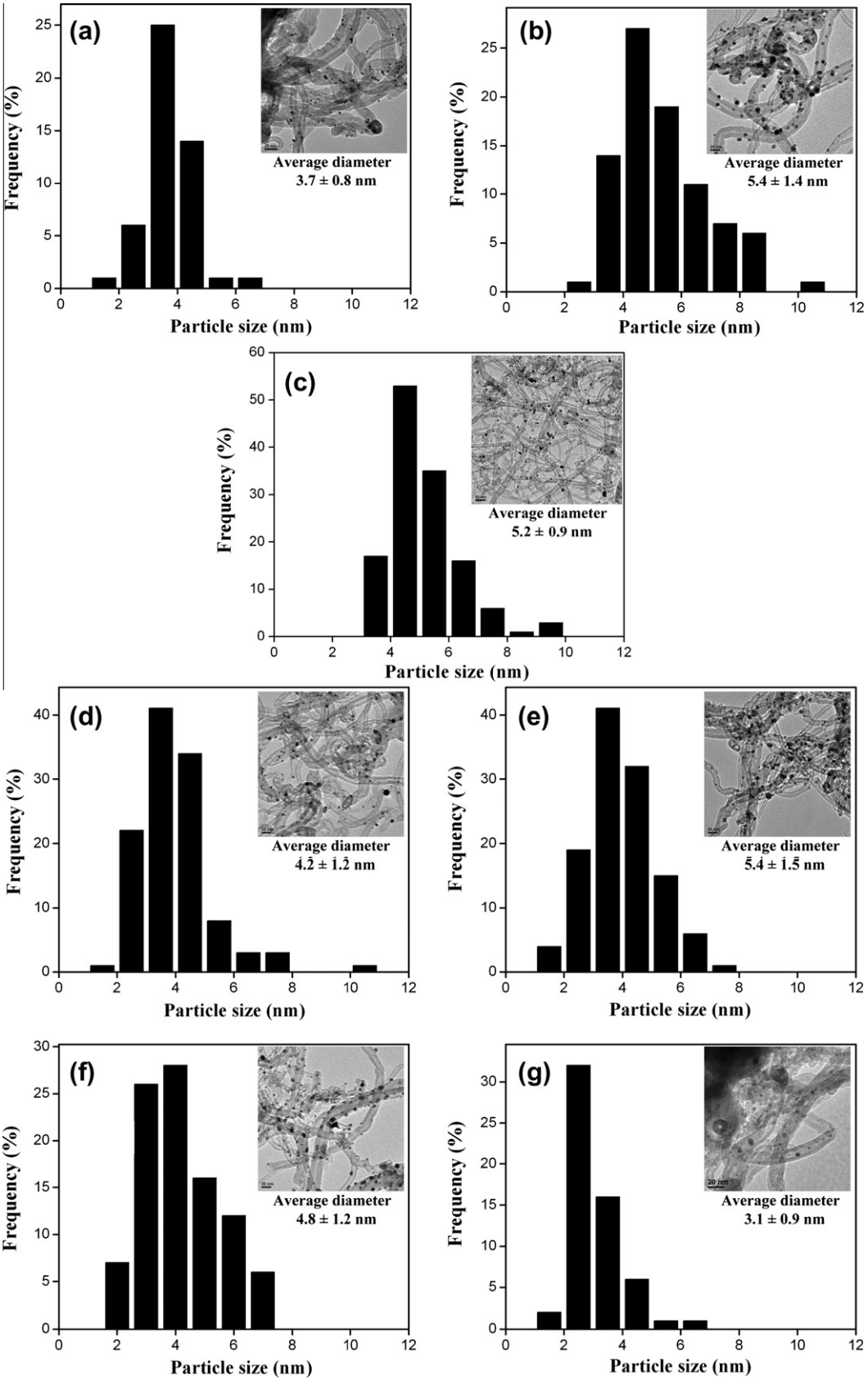

Fig. 4. TEM images and particle size distributions of: (a) Pt/CNT, (b) Pt/CNT-973, (c) Recycled Pt/CNT-973 after hydrogenation of CALD in 2-propanol at 333 K under 10 atm of hydrogen for 1 h; (d) PtFe/CNT-973, (e) PtCo/CNT-973, (f) PtFe/CNT-973-IMP and (g) PtCo/CNT-973-IMP, respectively.

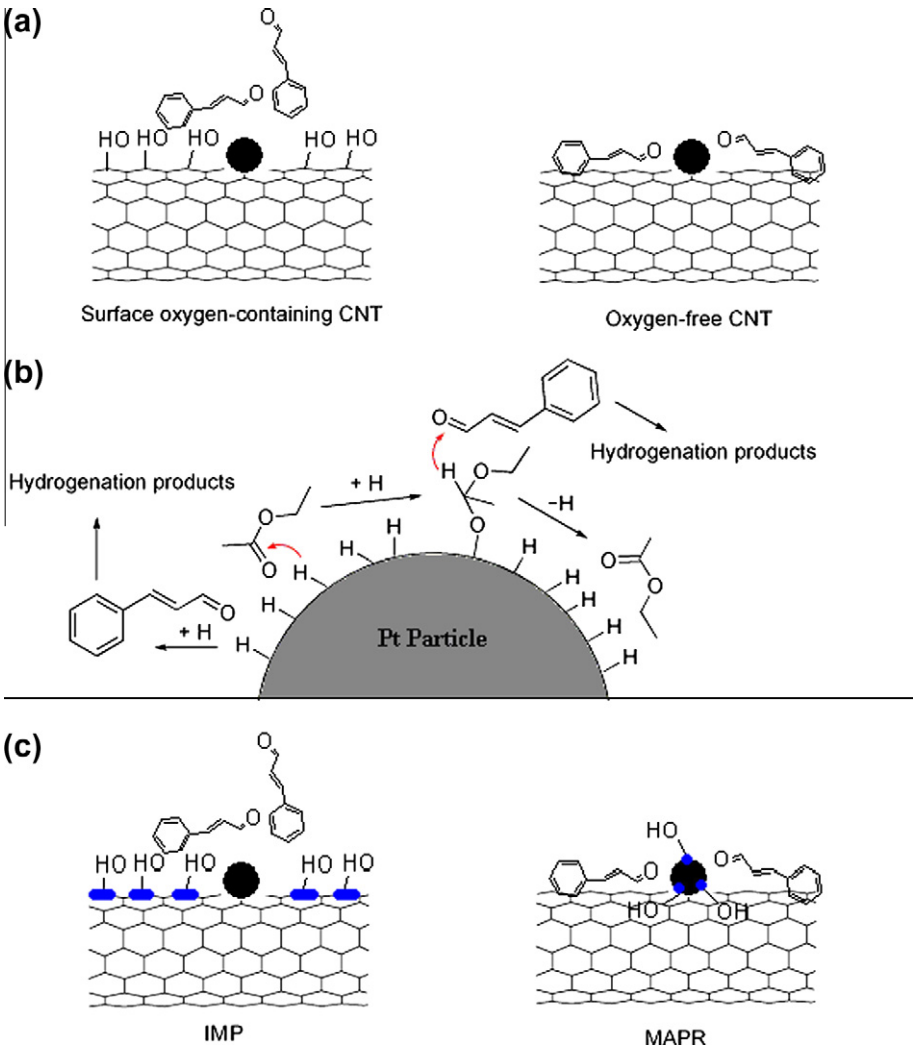

Scheme 1. (a) Hydrogenation of CALD on oxygen-containing CNT (left) and oxygen-free CNT (right) supported catalysts; (b) two hydrogenation pathways in EA; (c) hydrogenation of CALD on bimetallic catalysts synthesized using IMP (left) or MAPR (right) methods.

high temperature, the catalysts prepared by MAPR method were reduced in the liquid phase at a relatively low temperature. Therefore, compared to the catalyst prepared by IMP method, more oxygen-containing groups remain on CNT surfaces (evidenced by CV measurements of monometallic Pt/CNT and the corresponding impregnated catalyst Pt/CNT-IMP, as shown in Supporting information Fig. S-3), which may seriously impede the hydrogenation steps due to the acid sites on the CNT support surfaces.

Kinetic studies of CALD hydrogenation were investigated, and the results are shown in Fig. 5. At the initial stage of reaction (within 5 min), Pt/CNT-973 outperforms Pt/CNT-773, regardless of the similar amount of by-products formed over both catalysts. The superior activity of Pt/CNT-973 can be attributed to the removal of oxygen-containing groups from CNT surfaces, which enhances the π–π interaction between CALD and CNT. Nevertheless, the reaction rate over Pt/CNT-973 decreases gradually, which may be due to deactivation of catalytic sites caused by the deposition of carbonaceous by-products. The formation of carbonaceous deposits in the liquid catalytic system is referred as fouling which has been extensively investigated by Hajek et al. [34,35]. In a low-temperature reaction, the transformation of hydrocarbons does not occur, and the carbonaceous deposits are mostly non-desorbed [35]. However, further formation of by-products is inhibited to a large extent as a result of the hydrogenation steps and the rapid decrease in CALD concentration, as shown in Fig. 5. In case of Pt/CNT-773, constantly producing a large amount of by-products caused by the acid sites on CNT surfaces may exacerbate the catalyst deactivation. These results reveal that side reactions dominate the conversion of CALD over Pt/CNT-773, while the competition between hydrogenation and side reactions is observed over Pt/CNT-973.

Reasonable selectivity toward hydrogenation is obtained over Pt/CNT-873 and Pt/CNT-973, and the major hydrogenation product is CALC. These results further suggest that elimination of surface oxygen from CNT can facilitate the hydrogenation steps, especially the hydrogenation of C=O bond. Vu et al. suggested that the conductivity of CNT was improved by removing electronegative oxygen atoms from the CNT surface [10], which was further proved by the negatively shifted onset potential for CO oxidation in this study. The increased conductivity of CNT may enhance the electron transfer from CNT to metal active sites [10]. The enriched electron density surrounding the metallic nanoparticles reduces the probability of C=C bond coordinated to Pt active sites due to the electronic repulsion, thereby increases the selectivity toward CALC [10]. It is worth mentioning that the product distribution is different from the reported results over the Pt nanoparticles supported on CNF, in which the CALC selectivity decreased with the density of surface oxygen-containing groups on CNF, although both activity and selectivity toward total hydrogenation product were improved [19]. The Pt nanoparticle size for Pt/CNT-973 (5 nm) is

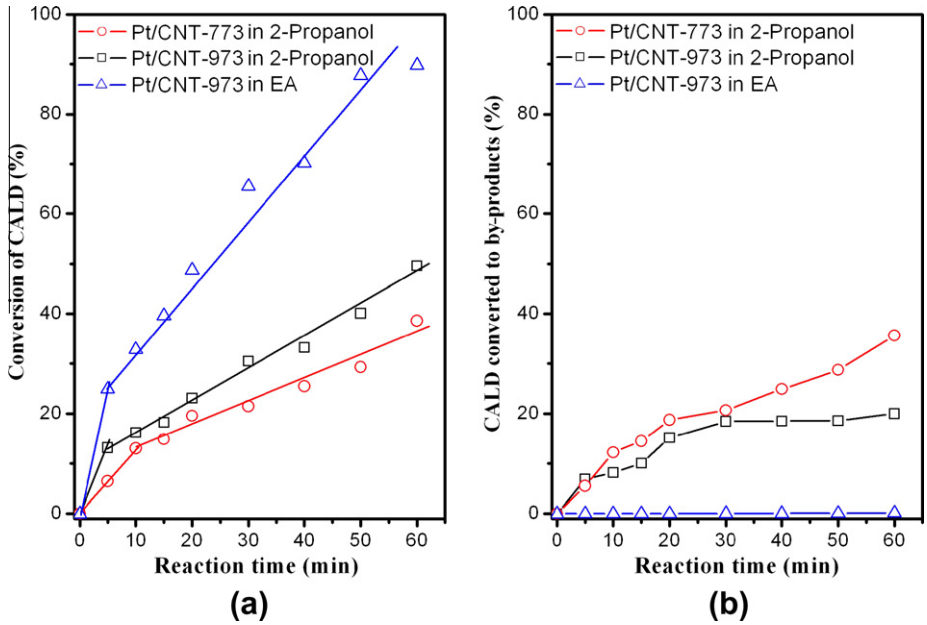

Fig. 5. Kinetic studies on hydrogenation of CALD over Pt/CNT-773 and Pt/CNT-973 by using either 2-propanol or EA as a solvent. (a) Conversion of CALD as a function of time; (b) percentage of CALD converted to by-products as a function of time.

larger than that of the catalyst reported by Toebes et al. (1–3 nm) [19], and it has been generally accepted that a slightly larger Pt nanoparticle size leads to a higher selectivity toward CALC due to the steric effect [3,18]. Furthermore, the curved graphite surface of CNT is beneficial to the charge transfer when compared to other carbon structures [36]. CNF is of a fishbone-type structure with the edges of graphite planes exposed at the surface [19]; the enhancement of electron transfer by removing surface oxygen is less pronounced for CNF due to the orientation of graphite layers and the hydrogen atoms at the external edges.

3.2. Effects of solvents

Compared to the large number of reports on designing effective catalysts, investigations into the solvent effect on CALD hydrogenation are limited [3]. The solvent plays a crucial role in this particular hydrogenation reaction; some solvents such as alcohols may be involved in the side reactions [19], and hydrocarbon solvents usually give a poor activity [3]. In this study, six solvents were examined for CALD hydrogenation over Pt/CNT-973, and the results are listed in Table 2. The hydrogenation activities and selectivities show a strong dependence on the selection of solvent. It was suggested that a polar solvent enhances the formation of products that are more polar than reactants [37]. The polarities of solvents in this study are of the following sequence: cyclohexane < EA < 1-butanol < ethanol < 2-propanol < dioxane. Both activity and selectivity toward CALC increase with solvent polarity due to the higher polarity of CALC than that of CALD [38]. No reaction took place in dioxane under the current hydrogenation conditions, implying that the catalyst may be poisoned by dioxane due to the solvent adsorption. A similar result was reported in a previous work; dioxane was strongly adsorbed on Ru surfaces, which was attributed to the interaction between surface noble metal atoms and the unshared electron pair donated by oxygen atoms of dioxane [39]. It was also suggested that Pt-based catalysts interacted more strongly with solvent than Ru-based catalysts [39]. Significant improvements in catalytic activity and selectivity were obtained when using EA as the solvent. EA outperforms other solvents and the TOF increases by a factor of 4 and 2 when compared to two commonly used solvents, cyclohexane and 2-propanol, respectively.

Solubility of hydrogen in the solvent may play a significant role in this catalytic reaction. The hydrogen solubility in EA is higher than any other alcohol employed in this study [40], which may partially contribute to the improved activity in EA. Although the hydrogen solubility in alcohols is proportional to the molecular weight of alcohols [40], a poor catalytic activity of hydrogenation

Table 2
Hydrogenation results of CALD over Pt/CNT-973 in different solvents.

Solvents	Conversion (%)	Yield of products (mol.%)				TOF[b] (h^{-1})
		CALC	HALD	HALC	Others[a]	
Cyclohexane	23.4	17.7	16.9	0	65.4	1062
Ethyl acetate	89.8	78.8	6.8	14.2	0.2	4079
1-Butanol	39.0	34.0	6.6	0	59.4	1771
Ethanol	64.9	47.6	5.2	0	47.2	2948
2-Propanol	49.6	55.1	4.6	0	40.3	2288
1,4-Dioxane	0	–	–	–	–	–

[a] Based on the characterization by GC–MS, the other by-products include 1-(3-propoxyprop-1-enyl)benzene, 1-((E)-3-propoxyprop-1-enyl)benzene, 1-(3-ethoxyhexa-1,5-dienyl)benzene, cinnamyl formate, cinnamic acid, benzyl cinnamate, 4,4-diphenylcyclohexa-1,5-dienyl acetate, 2-(hydroxy(phenyl)methyl)hexanal and some condensation products which cannot be identified by our MS due to their large molecular weights.

[b] TOF is defined as the number of converted CALD molecules in 1 h over one active site; the number of active sites (Pt atoms exposed on the surface of particles) is determined by EAS value. Reaction time is 1 h.

is observed in 1-butanol, which may be due to the low polarity of 1-butanol and the catalyst deactivation derived from the high selectivities toward by-products. High pressure increases the solubility of hydrogen in EA [40]. In this study, CALD hydrogenation in EA under different hydrogen pressures shows that high pressure leads to a high conversion along with an improved selectivity toward HALC rather than CALC (see Table 3). On the other hand, hydrogenation of CALD in EA over bared CNT after high-temperature (973 K) annealing under the same reaction conditions (10 atm of hydrogen, 333 K for 1 h) shows a conversion of 6.0% and 100% selectivity toward HALD. Similar results (5.9% of CALD conversion and 100% of HALD selectivity) are obtained when the reaction is performed in the absence of any catalyst, implying the lack of catalytic capability of CNT in this particular reaction. These results suggest that CALD hydrogenation in EA may undergo a distinct reaction pathway besides the direct hydrogenation of CALD by H atoms adsorbed on Pt nanoparticles.

Aiming at understanding the role of a solvent in the liquid phase reaction, the chemistry involving common organic solvents, e.g., esters, ethers and alcohols on Pt surfaces in the presence of H_2 has been investigated at room temperature using a reflection–absorption infrared spectroscopy (RAIRS) [41]. A small amount of CO adsorbed on Pt was detected due to the decomposition of ethanol. No CO adsorption was found when Pt was immersed in EA liquid film. As CO is notorious for its poison effect on Pt-based catalysts, the high stability of EA on Pt surfaces may partially explain why Pt/CNT-973 exhibits a remarkably high activity in EA. Investigations into EA hydrogenation revealed the formation of hemiacetal bonded on noble metal surfaces as an intermediate [42]. Herein, it is tentatively proposed that the hemiacetal intermediate may also form and participate in the CALD hydrogenation. As illustrated in Scheme 1b, when EA adsorbs on Pt nanoparticle, dissociated hydrogen adsorbed on Pt transfers to the carbonyl group of EA. The oxygen of carbonyl group subsequently bonds to a vacant Pt site to form the hemiacetal intermediates [42]. Further reduction of EA is not preferable because it occurs only at a substantially higher temperature [42]. Hydrogen transfer may occur from the unstable hemiacetal intermediate to CALD, leading to the transfer hydrogenation between CALD and the intermediate. This proposed mechanism may explain why both selectivity and activity remarkably increase in EA. Firstly, the competitive adsorption of CALD and EA solvent on Pt surfaces is not necessary for hydrogenation because the intermediate can transfer hydrogen to CALD. This may be the major factor accounting for the high TOF in EA. Secondly, it is also not surprising to observe that the selectivities toward by-products contributed by side reactions are extremely low (0.2%) due to the favorable hydrogenation of CALD in EA. The C=C double bond hydrogenation may also be suppressed due to the steric resistance between the intermediate and aryl ring of CALD, resulting in a high selectivity toward CALC. In contrast to the hydrogenation of CALD over Pt/CNT-973 in 2-propanol, detailed studies on the time-dependent catalytic behavior of Pt/CNT-973 in EA show that the CALD conversion is controlled by the hydrogenation steps (see Fig. 5). By changing the solvent from 2-propanol to EA, the reaction rate remarkably increases, which can be attributed to the enhanced hydrogenation rates and suppressed formation of by-products. Thus, the possibility of depositing carbonaceous by-products on catalytic sites is minimized.

As the commercial EA contains less than 0.2 wt.% of water, the influence of water content is also investigated by adding different amount of water in pre-dried EA (which is prepared by distillation of commercial EA on CaH_2). The results in Table 4 show that the activity over Pt/CNT-973 increases in the presence of a little amount of water in EA (<0.2 wt.%), followed by a rapid decrease due to the excess water content. Similar trend was also found in a ethanol–water system, in which the best result was obtained in the presence of 10 wt.% of water [43]. The remarkable difference is that even a trace amount of water (<0.2 wt.%) can influence the catalytic behavior dramatically in this study. Details of water effect are still under investigation.

3.3. Effects of promoters and preparation methods

Adding a second metal (or metal oxide) to a Pt-based catalyst as the promoter may influence the catalytic performance of this particular catalyst in CALD hydrogenation [3]. In this work, introducing the promoter was simply achieved by mixing Pt and promoter precursor solutions with CNT support prior to the microwave-assisted reduction. Several transition metals were screened, and the results are summarized in Table 5. Most of the promoters (Mn, Ni, Cu, Zn and Sn) show negative effects on CALD hydrogenation, whereas introducing Fe and Co improves CALC selectivity and CALD conversion, respectively. Fe- and Co-promoted Pt catalysts were also prepared by an IMP method and subsequently pretreated in nitrogen under a high temperature. As shown in Table 5, catalytic conversions dramatically decrease upon the impregnation of Fe and Co. The CALC selectivity remains constant for PtCo/CNT-973-IMP, and it decreases in the presence of impregnated Fe.

XRD patterns of these catalysts are shown in Fig. 3b; diffraction peaks assigned to the cubic platinum metal structure are clearly discernable. No reflections from Fe or Co metallic and oxidized species can be detected due to the low Fe and Co contents (1.47 and 1.56 wt.% for Fe and Co, respectively). The broadening of diffraction peaks for PtCo/CNT-973-IMP suggests the formation of relatively small Pt particles. Pt particle sizes for these samples are listed in Table 5; no clear correlation between particle size and preparation method can be derived. The mean particle sizes and size distributions were further measured by TEM observations, as shown in Fig. 4d–g. For the bimetallic catalysts synthesized by MAPR, the incorporation of Co affords a marginally larger Pt particle size

Table 3
Hydrogenation results of CALD over Pt/CNT-973 under different hydrogen pressures in EA at 333 K, reaction time: 1 h.

Pressure (atm)	Conversion (%)	Yield of products (mol.%)			
		CALC	HALD	HALC	Others[a]
5	71.5	81.0	8.8	10.0	0.2
10	89.8	78.8	6.8	14.2	0.2
15	98.4	64.5	4.0	31.4	0.1
20	99.8	40.4	1.4	58.0	0.2
30	100	23.9	0.8	75.2	0.1
40	100	19.2	0.5	80.1	0.2

[a] Based on the characterization by GC–MS, the other by-products include cinnamyl formate, cinnamic acid, 4,4-diphenylcyclohexa-1,5-dienyl acetate and some condensation products which cannot be identified by our MS due to their large molecular weights.

Table 4
Hydrogenation results of CALD over Pt/CNT-973 under 10 atm of hydrogen at 333 K in EA with different water contents, reaction time: 1 h.

Weight ratio of water (wt.%)	Conversion (%)	Yield of products (mol.%)			
		CALC	HALD	HALC	Others
0.0[a]	66.6	83.4	8.8	7.6	0.2
<0.2[b]	89.8	78.8	6.8	14.2	0.2
0.2	76.3	82.6	7.9	9.3	0.2
0.4	73.2	82.4	8.9	8.6	0.1
0.8	63.0	84.9	10.7	4.3	0.1
1.6	51.2	84.4	10.9	4.6	0.1

[a] The moisture-free EA was prepared by distillation of commercial EA over CaH_2.
[b] Based on the catalogue of commercial EA.

Table 5
Hydrogenation results of CALD over Pt-based bimetallic catalysts in EA.

Catalysts	Particle size (nm)	EAS ($m^{-2}\,g^{-1}$)	Conversion (%)	Yield of products (mol.%)				TOF[b] (h^{-1})
				CALC	HALD	HALC	Others[a]	
Pt/CNT-973	5.1	23.0	59.8	80.9	12.8	6.2	0.1	5433
PtMn/CNT-973	4.5	–	45.6	71.6	28.0	0.2	0.2	–
PtFe/CNT-973	4.5	15.1	56.5	87.7	11.5	0.7	0.1	7818
PtCo/CNT-973	5.0	19.0	66.2	73.8	18.4	7.7	0.1	7280
PtNi/CNT-973	5.3	–	53.4	76.5	20.4	3.0	0.1	–
PtCu/CNT-973	5.1	–	38.1	59.5	40.4	0	0.1	–
PtZn/CNT-973	4.8	–	41.7	77.1	21.3	1.4	0.2	–
PtSn/CNT-973	5.2	–	20.0	50.1	49.8	0	0.1	–
PtFe/CNT-973-IMP	4.9	28.6	11.9	66.3	33.6	0	0.1	869
PtCo/CNT-973-IMP	3.6	35.7	17.4	80.4	19.5	0	0.1	1018

[a] Based on the characterization by GC–MS, the other by-products include cinnamyl formate, cinnamic acid, 4,4-diphenylcyclohexa-1,5-dienyl acetate and some condensation products which cannot be identified by our MS due to their large molecular weighs.
[b] TOF is defined as the number of converted CALD molecules in 0.5 h over one active site; the number of active sites (Pt atoms exposed on the surface of particles) is determined by EAS value. Reaction time is 0.5 h.

and broader size distribution when compared to the Pt particles promoted by Fe. Nevertheless, the trend inverses for the impregnated catalysts; small particles with a narrow size distribution are formed on the Co-modified catalyst. These results imply that the interaction between Pt and promoter may be different due to the distinctive preparation strategies.

Most of the promoter precursors are nitrate salts, and the promoters should be present in the form of oxides if they are located on Pt surface and exposed to air. The available surface areas of Pt particles (represented by EAS areas derived from CO stripping measurements) are summarized in Table 5. In general, the EAS area is inversely proportional to the particle size of Pt monometallic catalyst. The same trend also applies to PtFe/CNT-973-IMP and PtCo/CNT-973-IMP; both impregnated catalysts have smaller particle sizes and larger EAS areas than Pt/CNT-973. Although the particle sizes of PtCo/CNT-973 (5.0 nm) and PtFe/CNT-973 (4.5 nm) are smaller than that of Pt/CNT-973, the active surface areas of Pt for these two catalysts are also lower than that of Pt/CNT-973 (see Table 5). We suggest that the small surface area is contributed by the coverage of Fe or Co oxides on Pt nanoparticles, namely a close contact between promoters and catalytic active centers. The significantly high TOF suggests the superior activity of surface Pt atoms for PtFe/CNT-973 and PtCo/CNT-973, while the relatively poorer conversion for PtFe/CNT-973 is attributed to the lower EAS area, i.e., fewer exposed Pt surface atoms. These observations imply that C=O bond activation in CALD hydrogenation is enhanced by the oxidized species attached on Pt surface as electrophilic or Lewis sites [3] because the electropositive oxides may adsorb and activate C=O bond via the unoccupied electron pair of oxygen. For the bimetallic catalysts prepared by IMP, promoters lack close contact with Pt, and adding the second metal does not have substantial influence on the EAS area, which can hardly contribute to the activation of C=O for hydrogenation (as illustrated in Scheme 1c). Furthermore, the metal oxide layer (or small clusters) deposited on CNT surfaces may hinder the adsorption of CALD via π–π interaction, resulting in the extremely low activities for impregnated bimetallic catalysts.

The CO stripping measurements show that the onset potentials for CO oxidation on PtFe/CNT-973 and PtCo/CNT-973 shift negatively (see Fig. 6), implying the promoted CO oxidization. The hydroxyl groups generated by water dissociation can adsorb on the surface of metal oxide species [44], and these adsorbed hydroxyls (OH_{ads}) may be involved in CO stripping and facilitate the oxidation of CO on a Pt surface [45]. Therefore, the negative shift of CO oxidization potential further demonstrates the close contact between metal oxide and Pt nanoparticles. On the contrary, the onset and peak potentials of CO oxidation for the impregnated catalysts are

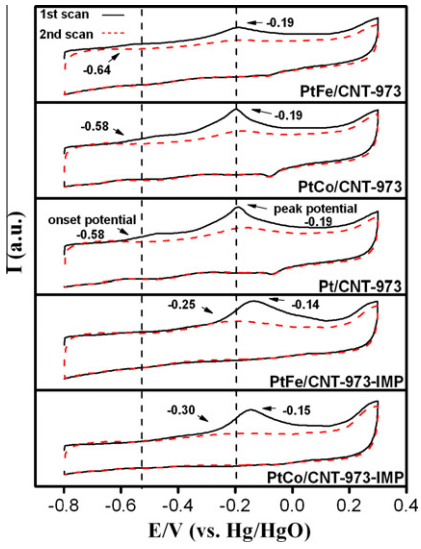

Fig. 6. CO stripping voltammograms of PtFe/CNT-973, PtCo/CNT-973, Pt/CNT-973, PtFe/CNT-973-IMP and PtCo/CNT-973-IMP. The left and right dash lines indicate the onset and peak potentials of Pt/CNT-973, respectively.

remarkably higher than Pt/CNT-973, as shown in Fig. 6, suggesting that impregnated Fe or Co mainly modifies the surface properties of CNT rather than Pt nanoparticles. The promoting effect of metal oxide on CO oxidization is based on the assumption that Pt particles are adjacent to the metal oxide promoters [45]. If the metal oxide locates apart from Pt active sites and disperses primarily on CNT surfaces, OH_{ads} can hardly participate in the CO oxidization due to the segregated distribution of Pt and metal oxide clusters (see Scheme 1c, left). The CNT conductivity may also be altered due to the coverage of metal oxide with OH_{ads}. Therefore, the CO oxidation is impeded by the decreased charge transfer capability of CNT, resulting in the positive shift of oxidization potential for impregnated catalysts.

CV profiles of these catalysts show that Pt–O reduction peak potentials for Fe- and Co-promoted catalysts prepared by MAPR shift negatively when compared to Pt/CNT-973, while Pt–O reduction peak potentials of corresponding impregnated bimetallic catalysts either remain constant or shift positively (see Fig. 7). Metal oxide islands on Pt nanoparticles may change the interaction between catalytic active sites and support, e.g., the electron flux from CNT to Pt nanoparticles under certain given potential. The current flow in response to applied potential may be diminished by metal

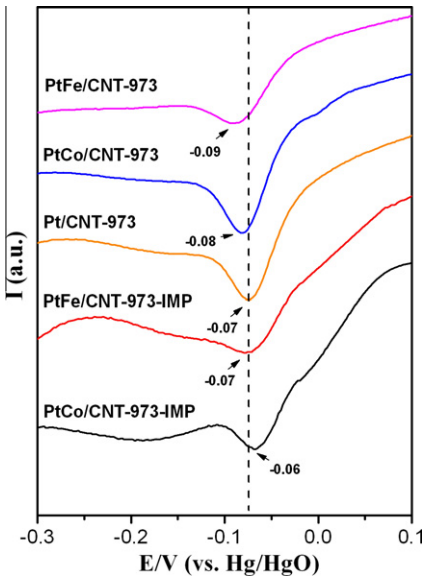

Fig. 7. Shift of Pt–O reduction peaks for PtFe/CNT-973, PtCo/CNT-973, PtFe/CNT-973-IMP and PtCo/CNT-973-IMP, comparing to Pt/CNT-973.

oxide species enriched on Pt particles, which decreases the number of available electrons for Pt–O reduction. For the impregnated bimetallic catalysts, the addition of promoters mainly contributes to the modification of support surface properties. Agglomeration of metal oxides with surface-adsorbed OH_{ads} decreases the conductivity of CNT support (evidenced by CO stripping), which may also impair the current flow toward Pt nanoparticles. Nevertheless, it also makes the catalyst surface more hydrophilic and more accessible to water, which facilitates the Pt–O reduction as interpreted in Eqs. (2) and (3), i.e., leading to a less negative reduction potential.

The existence of Co or Fe metallic phase alloyed with Pt after reduction cannot be completely ruled out in this one-step preparation and reduction. Therefore, two kinds of electron transfer mechanisms should be considered: one is from CNT support to metal active sites [10] the other is from promoter to Pt in the alloy [7,46]. Herein, XPS was employed to investigate the electron and oxidization states of Pt and promoters. To determine the peak position accurately, the XPS profiles were fitted by Gaussian–Lorentzian sum function (The fitting details are summarized in Supporting information Fig. S-4). As shown in Fig. 8a, Pt $4f_{7/2}$ binding energies of impregnated catalysts shift toward higher value when compared to those of Pt/CNT-973, suggesting that Fe or Co oxides dispersed on CNT surfaces may hinder the electron transfer from CNT to Pt, as donating electrons to Pt leads to the negative shift of Pt binding energy [14]. For bimetallic catalysts prepared by the MAPR method, Pt $4f_{7/2}$ binding energies are lower than those of Pt/CNT-973, which can be ascribed to the electron transfer from promoters to Pt due to the formation of alloy. The XPS spectra (Fig. 8b) show that nearly all the iron exists as metal oxide [47], and a shoulder peak at 707.85 eV is discernable for the Fe 2p spectrum of PtFe/CNT-973. This binding energy is slightly larger than $2p_{3/2}$ binding energy of metallic iron (706.8 eV) [47], which can be attributed to the formation of Pt–Fe alloy [48]. This shoulder peak is not obvious for PtFe/CNT-973-IMP. In the XPS spectra of Co 2p (Fig. 8c), the main peak centered at around 781 eV can be assigned to cobalt oxide species [49]. The broadening of cobalt peak for PtCo/CNT-973 may be due to the existence of metallic cobalt, which has the binding energy of *ca.* 778 eV [49].

In addition to the XPS measurements, an equilibrium adsorption constant of toluene and benzene ($K_{T/B}$) is used to characterize the electron density of Pt nanoparticles in the presence of promoters. $K_{T/B}$, which is derived from the relative hydrogenation rates of toluene and benzene (see Eq. (1)), is only correlated with reaction temperature and independent on other variables including particle size and support [17]. As the electron donation is easier for toluene compared to benzene, a larger $K_{T/B}$ value suggests a lower electron density of Pt nanoparticle [17]. As shown in Fig. 9, the lower $K_{T/B}$ value (3.24) of PtFe/CNT-973 when compared to that of Pt/CNT-973 (4.28) implies that electrons are transferred from Fe to Pt in this bimetallic catalyst. The increased electron density of Pt nanoparticles attenuates the binding energy, particularly that of C=C bond, and favors the hydrogenation of C=O [3]. The promoted CALC selectivity contributed by the electron transfer from iron to platinum was also detected by the X-ray absorption measurements

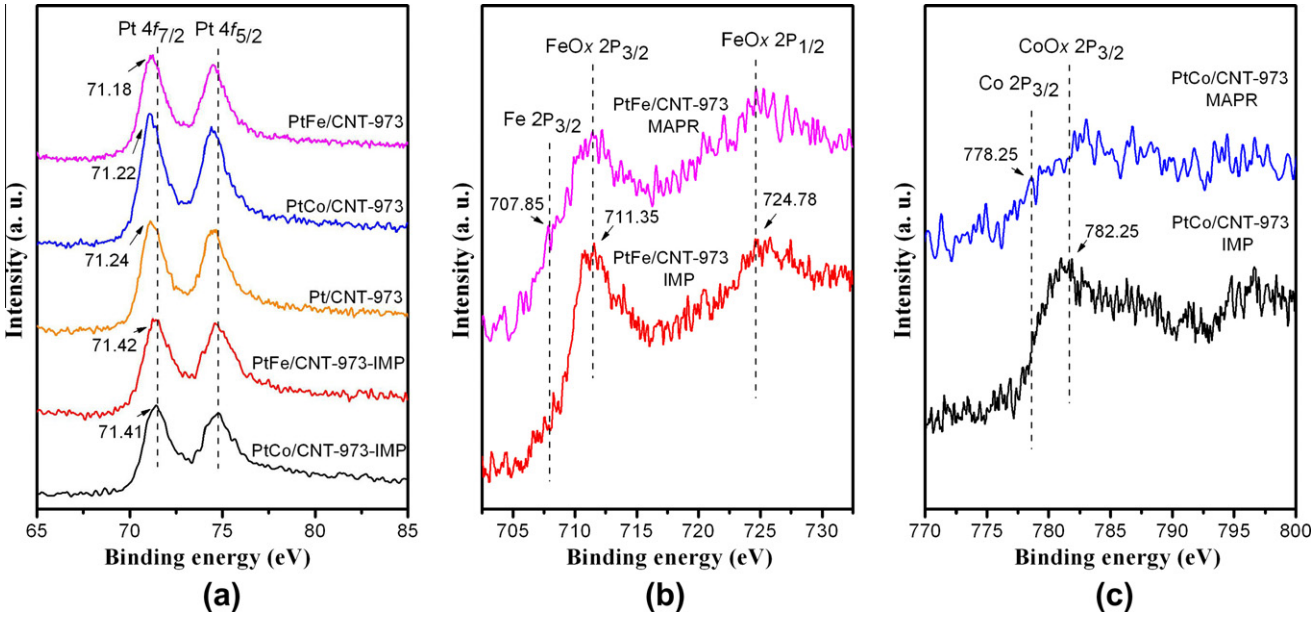

Fig. 8. XPS spectra of: (a) Pt, (b) Fe and (c) Co on Pt/CNT-973, PtFe/CNT-973, PtCo/CNT-973, PtFe/CNT-973-IMP and PtCo/CNT-973-IMP.

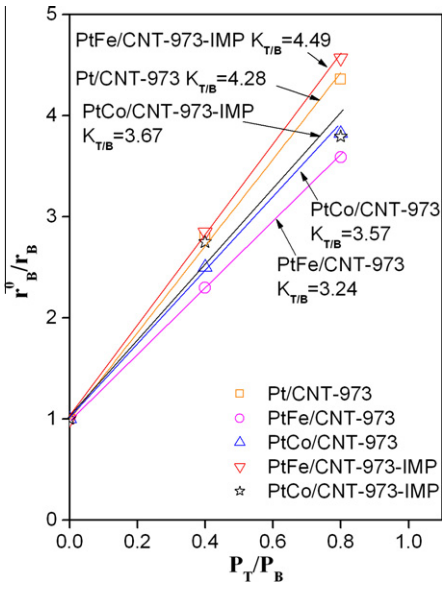

Fig. 9. Relative benzene hydrogenation rate vs. ratio of its partial pressure at 308 K. $K_{T/B}$ values of tested catalysts are slopes of lines.

on a carbon-supported Pt–Fe alloy [7]. The electron transfer from Co to Pt is relatively poorer as evidenced by the larger $K_{T/B}$ value for PtCo/CNT-973 (3.57). Less resistance toward the hydrogenation of C=C bonds leads to the formation of more HALD and HALC, which compromises the selectivity of CALC (see Table 5). For the impregnated catalysts, electron transfer from Co to Pt is also detected because of the lower $K_{T/B}$ value of PtCo/CNT-973-IMP (3.67). The discrepancy regarding the Pt 4f binding energy may be due to the low metal loadings. However, the electron transfer in PtCo/CNT-973-IMP is less pronounced when compared to PtCo/CNT-973, due to the lack of close contact between Co and Pt. For PtFe/CNT-973-IMP, the $K_{T/B}$ value (4.49) is even larger than that of Pt/CNT-973, implying that there is no electron transfer from Fe to Pt. Additionally, Fe species enriched on the support surface may hamper the electron transfer from CNT to Pt. The electron deficiency of Pt nanoparticles on PtFe/CNT-973-IMP promotes the formation of HALD and decreases the selectivity of CALC (see Table 5).

4. Discussion

It has been demonstrated that electrochemistry measurements including CV and CO stripping serve as complementary approaches to investigate the surface properties of CNT-supported catalysts. Based on the characterization and chemically probed reaction results, it can be concluded that surface oxygen-containing groups can be efficiently removed from CNT surfaces by the high-temperature treatment. Elimination of these groups suppresses acid-catalyzed side reactions and enhances the adsorption of CALD and electron transfer from CNT to Pt, resulting in substantially increased activity and selectivity to CALC. By screening various kinds of solvents, a dramatic increase in TOF as well as selectivity is observed when using EA as the solvent. It is proposed that in addition to the direct hydrogenation by H atoms adsorbed on Pt nanoparticles, transfer hydrogenation between CALD and EA occurs, in which EA can be partially reduced to afford a hemiacetal intermediate. Subsequent hydrogen transfer from this intermediate to CALD contributes to the high activity and selectivity.

The superior activity and selectivity for CALD hydrogenation over bimetallic catalysts synthesized by MAPR are ascribed to the close contact between promoters and Pt nanoparticles. The concept of "close contact" has been suggested by Plomp et al., in which the promoter (tin or gallium) was reduced by the hydrogen dissociated on pre-formed Pt particles [8]. Similarly, Co-decorated Pt nanoparticles were also synthesized by reducing Co in a suspension of Pt particles prepared in advance; an organic additive, 1,2-hexadecanediol, was employed as the reducing reagent [1]. Both examples require two successive reduction steps: one for the formation of Pt nanoparticles and the other for the reduction of promoters in the presence of Pt nanoparticles. In this microwave-assisted synthesis, the bimetallic catalysts with close contact between active sites and promoters can be prepared in one step. The reduction potential of platinum (1.188 V) is higher than that of iron (−0.440 V) and cobalt (−0.277 V) [50]; there is a high probability that Pt can be readily reduced by EG prior to the reduction of Fe or Co. It has been demonstrated that Co cannot be reduced in the absence of Pt particles when diol was the reducing agent [1]. Under a high temperature (433 K), EG may interact with Pt ions, resulting in the oxidation of EG to aldehyde, glycolic, oxalic acid or even CO_2. The electrons donated from these oxidation reactions lead to the reduction of Pt cations [12]. Once the Pt particles form, the oxidation of EG may take place via an alternative or parallel reaction pathway that involves the hydrogen abstraction from EG by platinum [12]. Thus, the hydrogen atoms adsorbed on Pt nanoparticles may facilitate the reduction and deposition of the second metal (Fe or Co) on Pt surfaces, which is similar to the reduction steps in the RDP method reported by Plomp et al. [8]. Further reductions of Pt and transition metal precursors afford the formation of alloys. Once the catalysts are exposed to air, Fe or Co metal on the Pt surface will be rapidly oxidized.

By employing the MAPR method, promoters are prone to closely interact with Pt active sites, which are essentially evidenced by CO stripping and CV measurements. The enrichment of promoters on Pt catalytic sites attains the hydrophobic surface of CNT which is beneficial to the adsorption of CALD reactants. In addition, the synergistic effects including activation of C=O bond and efficient metal-to-metal electron transfer (evidenced by $K_{T/B}$) remarkably enhance the catalytic activity and selectivity due to the close contact between Pt and promoter. For impregnated catalysts, promoters primarily disperse on the surface of CNT, which blocks the adsorption of CALD, resulting in low activities. Segregation of promoter and Pt active site diminishes the electron transfer from promoter to Pt, even hinders the electron donation from CNT to Pt. Pt nanoparticles with low electron density cannot efficiently inhibit the reduction of C=C bonds, resulting in a low selectivity toward CALC.

5. Conclusions

In this study, Pt-based mono- and bimetallic catalysts were synthesized by employing a facile and rapid MAPR method. These catalysts were successfully applied to the selective hydrogenation of CALD to CALC. The hydrogenation results highly depended on the surface properties of the CNT support, solvent and promoter. Removal of oxygen-containing groups from CNT surfaces elevated both activity and selectivity, due to the suppressed side reactions catalyzed by acid and enhanced electron transfer from CNT to Pt nanoparticles. By screening solvents with different polarities, EA was identified as the best candidate in this reaction, and the enhanced activity is hypothesized to result from the presence of parallel transfer hydrogenation steps. The catalytic properties can be promoted by Fe and Co. Compared to IMP preparation, MAPR not only served as a facile and time-saving synthesis methodology but also afforded close contact between promoters and Pt nanoparticles, which attains the affinity between CNT and CALD due to the

π–π interaction and assists the metal–metal electron transfer. These synergic effects contributed to the significantly improved activity and high selectivity.

Acknowledgment

Funding from the Singapore Agency for Science, Technology and Research (A*STAR), SERC Grant No: 102 101 0020 in support of this project is gratefully acknowledged.

Appendix A. Supplementary materials

Supplementary data associated with this article can be found, in the online version, at doi:10.1016/j.jcat.2010.09.021.

References

[1] S.C. Tsang, N. Cailuo, W. Oduro, A.T.S. Kong, L. Clifton, K.M.K. Yu, B. Thiebaut, J. Cookson, P. Bishop, ACS Nano 2 (2008) 2547.
[2] X.X. Han, R.X. Zhou, B.H. Yue, X.M. Zheng, Catal. Lett. 109 (2006) 157.
[3] P. Gallezot, D. Richard, Catal. Rev. 40 (1998) 81.
[4] Y. Li, C.H. Ge, J. Zhao, R.X. Zhou, Catal. Lett. 126 (2008) 280.
[5] M.A. Vannice, B. Sen, J. Catal. 115 (1989) 65.
[6] M. Englisch, A. Jentys, J.A. Lercher, J. Catal. 166 (1997) 25.
[7] A.B. da Silva, E. Jordao, M.J. Mendes, P. Fouilloux, Appl. Catal. A – Gen. 148 (1997) 253.
[8] A.J. Plomp, D.M.P. van Asten, A.M.J. van der Eerden, P. Maki-Arvela, D.Y. Murzin, K.P. de Jong, J.H. Bitter, J. Catal. 263 (2009) 146.
[9] W. Yu, Y. Wang, H. Liu, W. Zheng, J. Mol. Catal. A – Chem. 112 (1996) 105.
[10] H. Vu, F. Goncalves, R. Philippe, E. Lamouroux, M. Corrias, Y. Kihn, D. Plee, P. Kalck, P. Serp, J. Catal. 240 (2006) 18.
[11] C. Carnevillier, F. Epron, P. Marecot, Appl. Catal. A – Gen. 275 (2004) 25.
[12] C. Bock, C. Paquet, M. Couillard, G.A. Botton, B.R. MacDougall, J. Am. Chem. Soc. 126 (2004) 8028.
[13] S.L. Knupp, W. Li, O. Paschos, T.M. Murray, J. Snyder, P. Haldar, Carbon 46 (2008) 1276.
[14] N. Mahata, F. Goncalves, M.F.R. Pereira, J.L. Figueiredo, Appl. Catal. A – Gen. 339 (2008) 159.
[15] V. Lordi, N. Yao, J. Wei, Chem. Mater. 13 (2001) 733.
[16] D. Poondi, M. Albert Vannice, J. Catal. 161 (1996) 742.
[17] G.L. Haller, J. Catal. 216 (2003) 12.
[18] A.J. Plomp, H. Vuori, A.O.I. Krause, K.P. de Jong, J.H. Bitter, Appl. Catal. A – Gen. 351 (2008) 9.
[19] M.L. Toebes, Y.H. Zhang, J. Hajek, T.A. Nijhuis, J.H. Bitter, A.J. van Dillen, D.Y. Murzin, D.C. Koningsberger, K.P. de Jong, J. Catal. 226 (2004) 215.
[20] K.A. Wepasnick, B.A. Smith, J.L. Bitter, D.H. Fairbrother, Anal. Bioanal. Chem. 396 (2010) 1003.
[21] N.S. Lawrence, R.P. Deo, J. Wang, Electroanal 17 (2005) 65.
[22] H. Wang, R. Cote, G. Faubert, D. Guay, J.P. Dodelet, J. Phys. Chem. B 103 (1999) 2042.
[23] C.H. Hamann, A. Hamnett, W. Vielstich, Electrochemistry, Wiley-VCH, New York, 1998. p. 223.
[24] J.L. Cohen, D.J. Volpe, H.D. Abruna, Phys. Chem. Chem. Phys. 9 (2007) 49.
[25] F. Scholz, U. Schröder, R. Gulaboski, Electrochemistry of Immobilized Particles and Droplets, Springer, Heidelberg, 2005. p. 79.
[26] F. Maillard, M. Eikerling, O.V. Cherstiouk, S. Schreier, E. Savinova, U. Stimming, Faraday Discuss. 125 (2004) 357.
[27] E. Yoo, T. Okada, T. Kizuka, J. Nakamura, J. Power Sources 180 (2008) 221.
[28] Z.T. Liu, C.X. Wang, Z.W. Liu, J. Lu, Appl. Catal. A – Gen. 344 (2008) 114.
[29] S. Chytil, W.R. Glomm, E.A. Blekkan, Catal. Today 147 (2009) 217.
[30] W.Z. Li, C.H. Liang, W.J. Zhou, J.S. Qiu, Z.H. Zhou, G.Q. Sun, Q. Xin, J. Phys. Chem. B 107 (2003) 6292.
[31] U.M. Graham, A. Dozier, R.A. Khatri, M.C. Bahome, L.L. Jewell, S.D. Mhlanga, N.J. Coville, B.H. Davis, Catal. Lett. 129 (2009) 39.
[32] J.C. Duchet, E.M. van Oers, V.H.J. de Beer, R. Prins, J. Catal. 80 (1983) 386.
[33] Z.R. Li, Y.L. Fu, M. Jiang, T.D. Hu, T. Liu, Y.N. Xie, J. Catal. 199 (2001) 155.
[34] J. Hajek, J. Warna, D.Y. Murzin, Ind. Eng. Chem. Res. 43 (2004) 2039.
[35] J. Hajek, N. Kumar, T. Salmi, D.Y. Murzin, Catal. Today 100 (2005) 349.
[36] P.J. Britto, K.S.V. Santhanam, A. Rubio, J.A. Alonso, P.M. Ajayan, Adv. Mater. 11 (1999) 154.
[37] H. Rojas, J.L.G. Fierro, P. Reyes, J. Chil. Chem. Soc. 52 (2007) 1155.
[38] J. Hájek, N. Kumar, P. Mäki-Arvela, T. Salmi, D.Y. Murzin, J. Mol. Catal. A – Chem. 217 (2004) 145.
[39] H. Takagi, T. Isoda, K. Kusakabe, S. Morooka, Energy Fuels 13 (1999) 1191.
[40] M.S. Wainwright, T. Ahn, D.L. Trimm, N.W. Cant, J. Chem. Eng. Data 32 (1987) 22.
[41] Z. Ma, F. Zaera, Catal. Lett. 96 (2004) 5.
[42] O.A. Ferretti, J.P. Bournonville, G. Mabilon, G. Martino, J.P. Candy, J.M. Basset, J. Mol. Catal. 67 (1991) 283.
[43] Y.Z. Chen, S.W. Wei, K.J. Wu, Appl. Catal. A – Gen. 99 (1993) 85.
[44] Q. Yang, H. Choi, S.R. Al-Abed, D.D. Dionysiou, Appl. Catal. B – Environ. 88 (2009) 462.
[45] H. Yuan, D. Guo, X. Li, L. Yuan, W. Zhu, L. Chen, X. Qiu, Fuel Cell 9 (2009) 121.
[46] X. Wang, N. Li, L.D. Pfefferle, G.L. Haller, J. Phys. Chem. C (May) (2010), doi:10.1021/jp102511k.
[47] P.C.J. Graat, M.A.J. Somers, Appl. Surf. Sci. 100–101 (1996) 36.
[48] T. Ma, Q. Fu, Y. Cui, Z. Zhang, Z. Wang, D. Tan, X. Bao, Chin. J. Catal. 31 (2010) 24.
[49] M. Hakamada, K. Tajima, K. Yoshimura, Y. Chino, M. Mabuchi, J. Alloy. Compd. 494 (2010) 309.
[50] J.A. Dean, Lange's Handbook of Chemistry, McGraw-Hill, New York, 1999. p. 126.